

Growth of ZnO/Al₂O₃ Alloy Films Using Atomic Layer Deposition Techniques

J. W. Elam[†] and S. M. George^{*,†,‡}

Department of Chemistry and Biochemistry, and Department of Chemical Engineering,
University of Colorado, Boulder, Colorado 80309-0215

Received May 30, 2002. Revised Manuscript Received December 4, 2002

Atomic layer deposition (ALD) is an ideal technique for fabricating composite thin films. The thickness and stoichiometry of composite thin films prepared using ALD is dependent on the underlying surface chemistry during ALD film growth. A set of ZnO/Al₂O₃ alloy films was prepared by ALD in a viscous flow reactor using alternating Zn(CH₂CH₃)₂/H₂O exposures for ZnO ALD and alternating Al(CH₃)₃/H₂O exposures for Al₂O₃ ALD. The ZnO reaction cycle percentage was varied from 0 to 100%. The composite film thicknesses were measured using ex situ stylus profilometry and ellipsometry. The atomic composition of the composite films was established by atomic emission spectroscopy. Large deviations were found when the measured thicknesses and compositions were compared with “rule of mixtures” predictions. Many of the ZnO/Al₂O₃ alloy films showed lower than expected Zn film content and were thinner than predicted by the ALD growth rates of the pure ZnO and Al₂O₃ films. To understand these discrepancies, in situ quartz crystal microbalance measurements were performed during the ZnO/Al₂O₃ alloy film growth. The QCM measurements revealed that the Zn deficiency may result from the etching of Zn by the Al(CH₃)₃ precursor during the Al₂O₃ ALD cycles. In addition, the lower than expected film thicknesses are caused by a reduced initial growth rate for ZnO ALD on Al₂O₃ or Al-doped ZnO surfaces and Al₂O₃ ALD on ZnO or Zn-doped Al₂O₃ surfaces. A nucleation period of 4–6 cycles for ZnO ALD was observed following one or more Al₂O₃ reaction cycles. Similarly, a 2–3 cycle nucleation period was monitored for Al₂O₃ ALD following the ZnO reaction cycles. Understanding the underlying surface chemistry during ALD helps predict the thickness and composition of composite thin films grown using ALD techniques.

I. Introduction

Composite thin films may be fabricated by co-depositing two or more materials. The component materials may be combined in alternating, discrete layers to form multilayered laminates. Alternatively, the composite materials may be homogeneously blended to form alloys. A wide range of physical properties may be achieved by varying the relative proportions of the components. This strategy has been used previously to control numerous thin film properties including refractive index,¹ dielectric constant,² lattice constant,³ hardness,⁴ charge storage capacity,⁵ and surface roughness.⁶

Atomic layer deposition (ALD) is a useful technique for constructing composite thin films. ALD utilizes sequential, self-limiting surface chemical reactions to

achieve atomic layer controlled thin film growth.^{7,8} Films grown using ALD are typically dense, pinhole-free, and extremely conformal to the underlying substrate. ALD methods have been employed previously to deposit a wide variety of novel composite materials including nanolaminates,^{1,5,9–16} alloys,^{2,3,17–28} mixed oxides,^{29–31} and doped materials.^{32–37}

* To whom correspondence should be addressed. Phone: 303-492-3398. Fax: 303-492-5894. E-mail: georges@spot.colorado.edu.

[†] Department of Chemistry and Biochemistry.

[‡] Department of Chemical Engineering.

(1) Kattelus, H.; Ylilammi, M.; Saarilahti, J.; Antson, J.; Lindfors, S. *Thin Solid Films* **1993**, *225*, 296.

(2) Stromme, M.; Niklasson, G. A.; Ritala, M.; Leskela, M.; Kukli, K. *J. Appl. Phys.* **2001**, *90*, 4532.

(3) Fujiwara, H.; Nabeta, T.; Shimizu, I. *Jpn. J. Appl. Phys.* **1994**, *33*, 2474.

(4) Chu, X.; Wong, M. S.; Sproul, W. D.; Barnett, S. A. *J. Mater. Res.* **1999**, *14*, 2500.

(5) Kukli, K.; Ritala, M.; Leskela, M. *J. Appl. Phys.* **1999**, *86*, 5656.

(6) Elam, J. W.; Sechrist, Z. A.; George, S. M. *Thin Solid Films* **2002**, *414*, 43.

(7) Suntola, T.; Hyvarinen, J. *Ann. Rev. Mater. Sci.* **1985**, *15*, 177.

(8) George, S. M.; Ott, A. W.; Klaus, J. W. *J. Phys. Chem.* **1996**, *100*, 13121.

(9) Ritala, M.; Leskela, M.; Niinisto, L.; Prohaska, T.; Friedbacher, G.; Grasserbauer, M. *Thin Solid Films* **1994**, *249*, 155.

(10) Kukli, K.; Ihanus, J.; Ritala, M.; Leskela, M. *Appl. Phys. Lett.* **1996**, *68*, 3737.

(11) Hartmann, J. M.; Charleux, M.; Mariette, H.; Rouviere, J. L. *Appl. Surf. Sci.* **1997**, *112*, 142.

(12) Ishii, M.; Iwai, S.; Kawata, H.; Ueki, T.; Aoyagi, Y. *J. Cryst. Growth* **1997**, *180*, 15.

(13) Kumagai, H.; Toyoda, K.; Kobayashi, K.; Obara, M.; Iimura, Y. *Appl. Phys. Lett.* **1997**, *70*, 2338.

(14) Zhang, H.; Solanki, R.; Roberds, B.; Bai, G.; Banerjee, I. *J. Appl. Phys.* **2000**, *87*, 1921.

(15) Kukli, K.; Ritala, M.; Leskela, M. *J. Electrochem. Soc.* **2001**, *148*, F35.

(16) Zhang, H.; Solanki, R. *J. Electrochem. Soc.* **2001**, *148*, F63.

(17) McDermott, B. T.; Reid, K. G.; El-Masry, N. A.; Bedair, S. M.; Duncan, W. M.; Yin, X.; Pollak, F. H. *Appl. Phys. Lett.* **1990**, *56*, 1172.

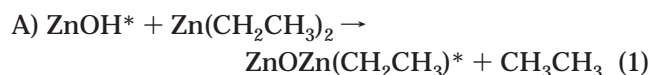
(18) Fujiwara, H.; Nabeta, T.; Kiryu, H.; Shimizu, I. *Jpn. J. Appl. Phys.* **1994**, *33*, 4381.

(19) Asikainen, T.; Ritala, M.; Leskela, M. *J. Electrochem. Soc.* **1995**, *142*, 3538.

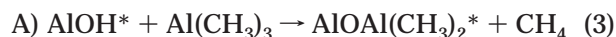
(20) Boutros, K. S.; McIntosh, F. G.; Roberts, J. C.; Bedair, S. M.; Piner, E. L.; El-Masry, N. A. *Appl. Phys. Lett.* **1995**, *67*, 1856.

Composite films can be fabricated by adjusting the ALD pulse sequence. During the ALD of material KL, the K and L reactive precursor gases are injected into the ALD reactor in an ABAB... sequence. To perform ALD of a composite mixture of KL and MN materials, a pulse sequence can be employed using (KL)_X(MN)_Y.... In this pulse sequence, the ratio *X/Y* establishes the stoichiometry of the composite material and the magnitudes of *X* and *Y* determine whether the resulting film is a nanolaminate or alloy. For example, if both *X* and *Y* are large compared with the number of KL or MN cycles required to deposit full monolayers of these materials, then the (KL)_X(MN)_Y... pulse sequence will create a nanolaminate with distinct KL and MN layers. However, if *X* and *Y* are both small, the pulse sequence will generate a homogeneous alloy film.

This study investigates the growth of ZnO/Al₂O₃ alloy films using atomic layer deposition techniques. ZnO ALD is performed using alternating Zn(CH₂CH₃)₂ and H₂O exposures:^{38–41}



where the asterisks represent the surface species. By repeating these reactions in an ABAB... sequence, ZnO films can be deposited with atomic layer control. Al₂O₃ ALD is performed using alternating Al(CH₃)₃ and H₂O exposures:^{42–46}



Al₂O₃ films can be deposited with atomic layer control by repeating these reactions in an ABAB... sequence.

ZnO/Al₂O₃ alloy films are excellent for exploring the fabrication and properties of alloys using atomic layer deposition. These two materials exhibit very different physical properties. ZnO grown by ALD techniques is conducting, crystalline, and rough.^{38–41} In contrast, Al₂O₃ grown by ALD techniques is insulating, amorphous, and smooth.^{42–46} Consequently, composite mixtures of these two oxides may span a broad range of properties. To grow ZnO/Al₂O₃ alloy films that vary widely in composition, the percentage of ZnO reaction cycles was varied from 0 to 100%. The films were then analyzed using ex situ stylus profilometry, ellipsometry, and atomic emission spectroscopy. In situ quartz crystal microbalance measurements were also performed to explore the details of the ZnO/Al₂O₃ growth process.

II. Experimental Section

A. Viscous Flow Reactor for Atomic Layer Deposition.

The ZnO/Al₂O₃ alloy films were prepared in a viscous flow ALD reactor.⁴⁷ A schematic of this reactor is shown in Figure 1. The reactor is constructed from stainless steel components. The sample substrates are held in a stainless steel tube with an inside diameter of 3.5 cm. Ultrahigh purity nitrogen carrier gas transports the reactive precursors to the sample substrates and carries the reaction products and surplus reactants into the mechanical pump. The carrier gas is purified using an Aeronex Gate Keeper filter before entering the flow tube. The nitrogen flow rate is 200 sccm and the nitrogen velocity and the steady-state pressure in the flow tube are ~2.5 m/s and ~1 Torr, respectively.

The flow tube is heated resistively to the desired deposition temperature. The temperature is regulated using a PID Labview program running on a personal computer. The sample substrates and the in situ quartz crystal microbalance (QCM) are heated by radiation and convection from the tube walls. The substrates are HF-etched, loaded, and removed from the reactor within a class 100 laminar clean-room environment to prevent particulate contamination.

Pulses of the reactive precursors are injected into the nitrogen carrier gas flow using computer-controlled solenoid valves.⁴⁷ The amplitudes of the precursor pulses are adjusted to yield a pressure transient of $\Delta P \sim 0.1$ Torr using needle valves. The precursor sources are Akzo Nobel semiconductor grade trimethyl aluminum (TMA) and diethyl zinc (DEZ) and Fisher Optima purity deionized water. The ALD films were deposited on 1 in. \times 1 in. Si(100) substrates. Prior to loading, the samples were degreased using a 15-min dip in a piranha solution containing 70 mL of H₂SO₄ and 30 mL of 30% H₂O₂ in H₂O. Subsequently, the sample substrates were etched in a clean-room grade, 5% HF/H₂O solution for 1 min.

The films were deposited at 177 °C using reactant exposure times of 1 s and purge times of 3–5 s between exposures. Figure 2 shows a diagram of the reactant pulse sequence employed to deposit a ZnO/Al₂O₃ alloy film where 67% of the metal alkyl pulses are diethyl zinc pulses. The DEZ and H₂O pulses alternate during the deposition of the film. By substituting every third DEZ pulse with a TMA pulse, the resulting

- (21) Ihanus, J.; Ritala, M.; Leskela, M.; Rauhala, E. *Appl. Surf. Sci.* **1997**, *112*, 154.
- (22) Seim, H.; Nieminen, M.; Niinisto, L.; Fjellvag, H.; Johansson, L.-S. *Appl. Surf. Sci.* **1997**, *112*, 243.
- (23) Seim, H.; Molsa, H.; Nieminen, M.; Fjellvag, H.; Niinisto, L. *J. Mater. Chem.* **1997**, *7*, 449.
- (24) Nilsen, O.; Peussa, M.; Fjellvag, H.; Niinisto, L.; Kjekshus, A. *J. Mater. Chem.* **1999**, *9*, 1781.
- (25) Vehkamäki, M.; Hatanpää, T.; Hanninen, T.; Ritala, M.; Leskela, M. *Electrochem. Solid-State Lett.* **1999**, *2*, 504.
- (26) Song, J. H.; Sim, E. D.; Baek, K. S.; Chang, S. K. *J. Cryst. Growth* **2000**, *214*, 460.
- (27) Schuisky, M.; Kukli, K.; Ritala, M.; Harsta, A.; Leskela, M. *Chem. Vap. Deposition* **2000**, *6*, 139.
- (28) Juppo, M.; Alen, P.; Ritala, M.; Leskela, M. *Chem. Vap. Deposition* **2001**, *7*, 211.
- (29) Haukka, S.; Lindblad, M.; Suntola, T. *Appl. Surf. Sci.* **1997**, *112*, 23.
- (30) Nieminen, M.; Sajavaara, T.; Rauhala, E.; Putkonen, M.; Niinisto, L. *J. Mater. Chem.* **2001**, *11*, 2340.
- (31) Rahtu, A.; Hanninen, T.; Ritala, M. *J. Phys. IV* **2001**, *11*, 923.
- (32) Suntola, T.; Jorma, A. Method for Producing Compound Thin Films. U.S. Patent 4058430, 1977.
- (33) Virola, H.; Niinisto, L. *Thin Solid Films* **1994**, *251*, 127.
- (34) Kong, W.; Fogarty, J.; Solanki, R. *Appl. Phys. Lett.* **1994**, *65*, 670.
- (35) Elers, K.-E.; Ritala, M.; Leskela, M.; Rauhala, E. *Appl. Surf. Sci.* **1994**, *82/83*, 468.
- (36) Jung, D.; Leonard, M.; El-Masry, N. E.; Bedair, S. M. *J. Electron. Mater.* **1995**, *24*, 75.
- (37) Yousfi, E. B.; Weinberger, B.; Donsanti, F.; Cowache, P.; Lincot, D. *Thin Solid Films* **2001**, *387*, 29.
- (38) Lujala, V.; Skarp, J.; Tammenmaa, M.; Suntola, T. *Appl. Surf. Sci.* **1994**, *82/83*, 34.
- (39) Yamada, A.; Sang, B.; Konagai, M. *Appl. Surf. Sci.* **1997**, *112*, 216.
- (40) Ott, A. W.; Chang, R. P. H. *Mater. Chem. Phys.* **1999**, *58*, 132.
- (41) Yousfi, E. B.; Fouache, J.; Lincot, D. *Appl. Phys. Lett.* **2000**, *153*, 223.
- (42) Ott, A. W.; Klaus, J. W.; Johnson, J. M.; George, S. M. *Thin Solid Films* **1997**, *292*, 135.
- (43) Higashi, G. S.; Fleming, C. G. *Appl. Phys. Lett.* **1989**, *55*, 1963.
- (44) Ritala, M.; Saloniemi, H.; Leskela, M.; Prohaska, T.; Friedbacher, G.; Grasserbauer, M. *Thin Solid Films* **1996**, *286*, 54.

- (45) Ericsson, P.; Bengtsson, S.; Skarp, J. *Microelectron. Eng.* **1997**, *36*, 91.

- (46) Matero, R.; Rahtu, A.; Ritala, M.; Leskela, M.; Sajavaara, T. *Thin Solid Films* **2000**, *368*, 1.

- (47) Elam, J. W.; Groner, M. D.; George, S. M. *Rev. Sci. Instrum.* **2002**, *73*, 2981.

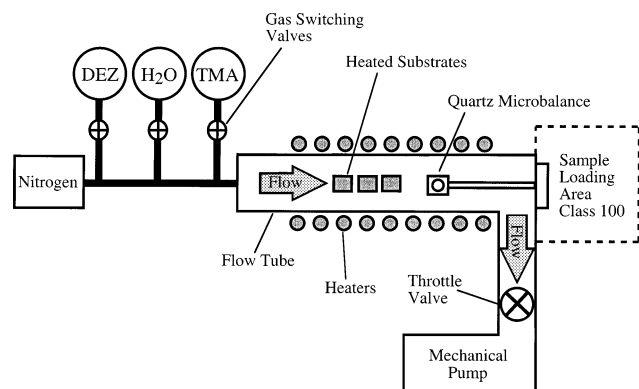


Figure 1. Schematic view of viscous flow reactor for atomic layer deposition (ALD).

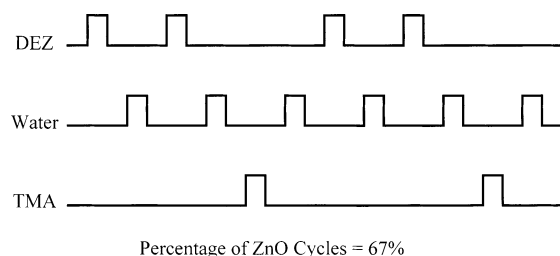


Figure 2. ALD pulse sequence for depositing ZnO/Al₂O₃ alloy film where the percentage of ZnO cycles is 67%.

ZnO/Al₂O₃ alloy film is as homogeneous as possible while maintaining the 67% ZnO cycle percentage.

B. In Situ Quartz Crystal Microbalance. The viscous flow ALD reactor is equipped with an in situ quartz crystal microbalance (QCM). Polished QCM sensors were obtained from Colorado Crystal Corporation (Part CCAT1BK-1007-000). These QCM sensors were mounted in a Maxtek BSH-150 bakeable sensor head attached to a 2.75-in. conflat flange. The sensor head was modified to provide an ~20 sccm nitrogen flow over the back surface of the sensor crystal. This nitrogen flow prevents deposition on the back of the sensor crystal.

Signals from the QCM sensor were measured by a Maxtek TM400 film thickness monitor interfaced to a computer. The thickness monitor and interface allowed mass measurements with 0.375 ng/cm² resolution to be performed every 0.1 s. Assuming a ZnO density of 5.61 g/cm³, this mass resolution equates to a thickness resolution for ZnO of 0.007 Å. Prior to recording QCM measurements, an Al₂O₃ buffer layer was deposited using several hundred TMA/H₂O cycles. This buffer layer converts the gold QCM surface to an Al₂O₃ surface. This Al₂O₃ buffer layer avoids any possible complications caused by the different nucleation and growth of ZnO and Al₂O₃ on gold.

C. Ex Situ Measurements. Thickness measurements of the ZnO/Al₂O₃ alloy films were performed using a Dektak 3 stylus profilometer and a Rudolph Research Auto EL ellipsometer. Steps for the profilometer were created in the alloy films using one of two methods. For the higher Zn percentage films, a line of Shipley AZ5214E photoresist was applied on top of the alloy film and cured by baking at 100 °C for 60 s. The unprotected oxide was then etched away in 10% nitric acid. Subsequently, the photoresist was removed by sonicating the film in acetone.

The ZnO/Al₂O₃ alloy films containing ≥25% Al were found to be insoluble in 10% nitric acid. Although these films could be dissolved in hydrofluoric acid, the HF also dissolved the photoresist. Consequently, a spot of Shipley AZ5214E photoresist was placed on the Si(100) substrates prior to film growth. After deposition of the alloy films, the photoresist was removed by rubbing it with an acetone-soaked cotton swab.

Elemental analysis was performed on the ZnO/Al₂O₃ alloy films by first dissolving a portion of each of the films in a 5% hydrofluoric acid/water mixture. The solutions were subse-

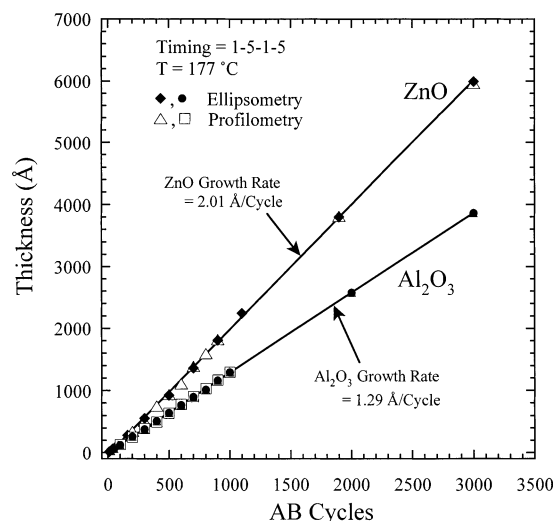


Figure 3. Thickness versus AB cycles for ZnO and Al₂O₃ ALD films deposited on HF-etched Si(100) substrates measured using ellipsometry (solid symbols) and stylus profilometry (open symbols).

quently analyzed by inductively coupled plasma (ICP) atomic emission spectroscopy (AES). The Zn film content was evaluated using

$$\text{Zn Film Content (\%)} = \left[\frac{\text{Zn}}{(\text{Zn} + \text{Al})} \right] \times 100 \quad (5)$$

where Zn and Al are the amounts of these elements present in the film as determined by the ICP AES measurements.

III. Results

A. Pure ZnO and Al₂O₃ ALD Films. Figure 3 presents the thicknesses measured for the pure ZnO and Al₂O₃ ALD films. A linear least-squares fit to the ZnO thickness measurements yields an average ZnO ALD growth rate of 2.01 Å/cycle. Similarly, a linear least-squares fit to the Al₂O₃ thickness data yields an average growth rate for Al₂O₃ ALD of 1.29 Å/cycle.

The growth rates for the ZnO and Al₂O₃ ALD films change slightly with the number of AB cycles. Figure 4 presents the ZnO and Al₂O₃ ALD growth rates determined by dividing the thickness measurements in Figure 3 by the corresponding numbers of AB cycles. The error bars on the open triangles and open squares represent the standard deviations obtained from stylus profilometric measurements at 4–5 different locations on the ALD films. The ZnO ALD growth rate increases from ~1.5 Å/cycle at 10 cycles and saturates at 2.01 Å/cycle after 700–900 cycles. The Al₂O₃ ALD growth rate is nearly constant at 1.29 Å/cycle. However, the ellipsometry data suggests a slightly lower Al₂O₃ ALD growth rate of 1.05 Å/cycle at 25 AB cycles.

Figure 5 presents in situ quartz crystal microbalance (QCM) measurements recorded during the ALD of pure ZnO and Al₂O₃ films. A linear least-squares fit to the ZnO QCM data indicates a ZnO ALD growth rate of 113 ng/cm²/cycle. Assuming a bulk ZnO density of 5.6 g/cm³, this equates to a ZnO ALD growth rate of 2.0 Å/cycle. The Al₂O₃ QCM data yields an Al₂O₃ ALD growth rate of 37.6 ng/cm²/cycle. The Al₂O₃ ALD growth rate is 1.3 Å/cycle assuming an Al₂O₃ density of 2.9 g/cm³ as discussed in Section IV.A.

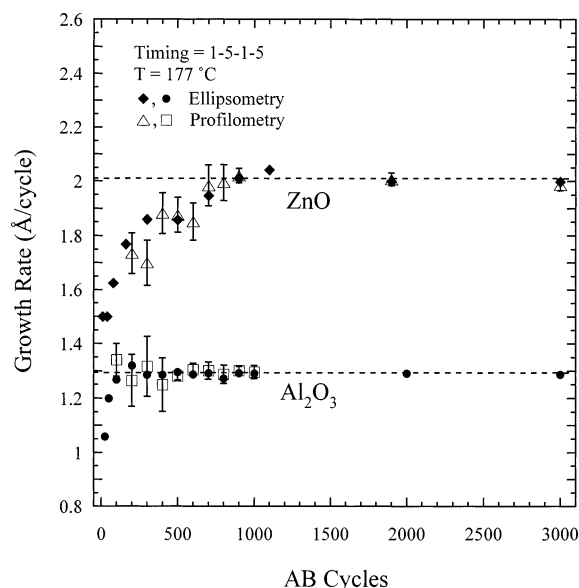


Figure 4. Growth rates for ZnO and Al₂O₃ ALD versus number of AB cycles determined by dividing the thickness measurements in Figure 3 by the corresponding numbers of AB cycles.

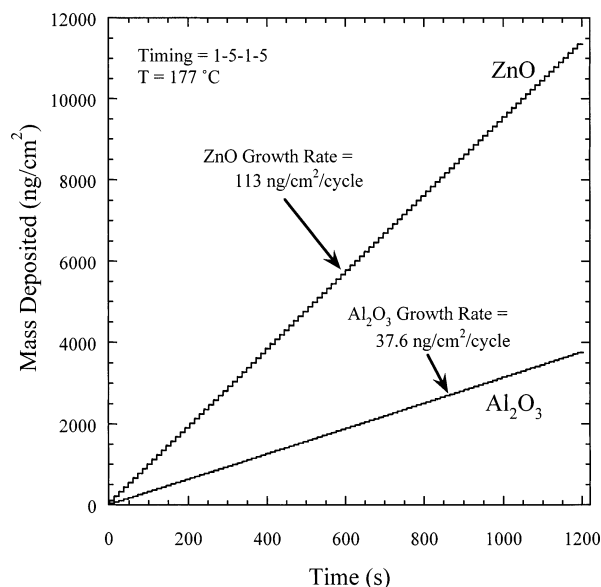


Figure 5. In situ quartz crystal microbalance (QCM) measurements for 100 AB cycles of ZnO and Al₂O₃ ALD.

Figure 6 presents the average QCM pulse shapes for the measurements in Figure 5 and shows the average mass change occurring during the individual ZnO and Al₂O₃ ALD cycles. The status of the metal alkyl and H₂O exposures during the ALD of the ZnO and Al₂O₃ films is indicated by the dashed lines. Figure 6a demonstrates that virtually all of the ZnO mass is added to the surface during the DEZ pulse. Similarly, Figure 6b shows that nearly all of the Al₂O₃ mass is added to the surface during the TMA pulse. The ΔM_A and $\Delta M_A + \Delta M_B$ quantities in Figure 6 are discussed in Section IV.A.

B. ZnO/Al₂O₃ Alloy ALD Films. Figure 7 displays the Zn film content for a set of ZnO/Al₂O₃ ALD alloy films determined using ICP AES measurements versus the percentage of ZnO cycles. This percentage is expressed by the quantity $[\text{DEZ}/(\text{DEZ} + \text{TMA})] \times 100$ where DEZ and TMA are the numbers of diethyl zinc

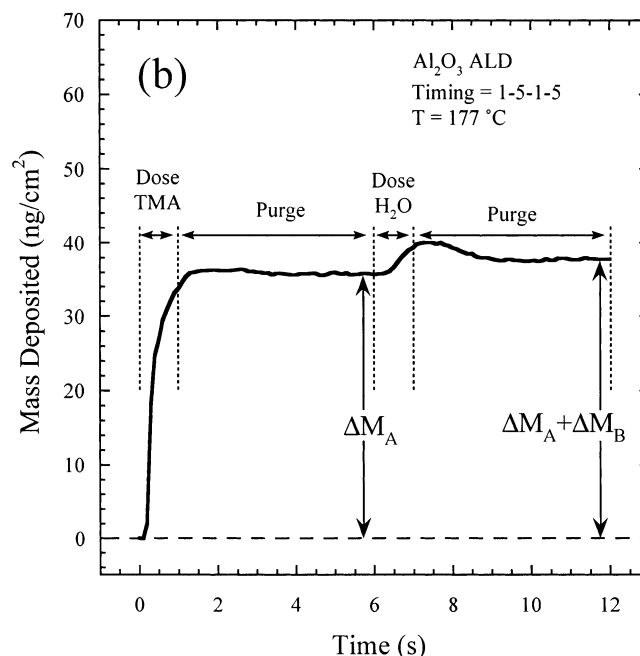
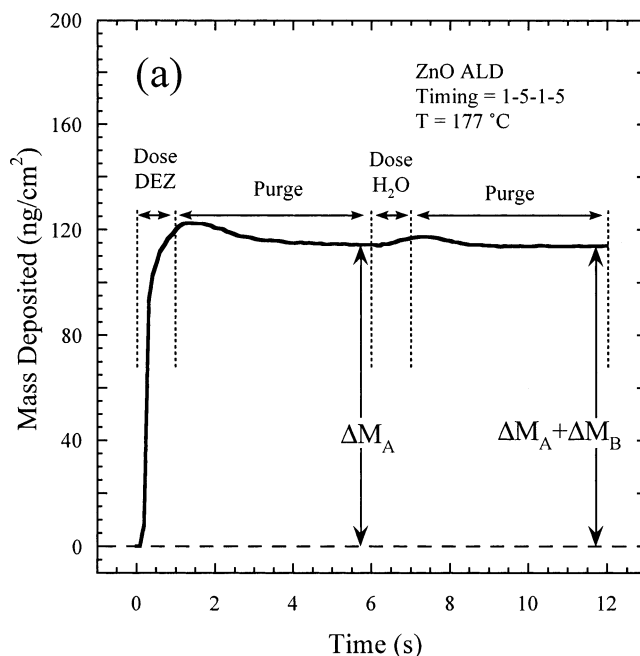


Figure 6. Average QCM pulse shapes for (a) ZnO ALD and (b) Al₂O₃ ALD.

and trimethyl aluminum pulses applied as illustrated in Figure 2. The dashed line in Figure 7 shows the Zn film content expected for a given percentage of ZnO cycles calculated using the “rule of mixtures” formula:

$$\text{Zn Film Content (\%)} = \left[\frac{\rho_{\text{Zn}} \% \text{ZnO}}{\rho_{\text{Zn}} \% \text{ZnO} + \rho_{\text{Al}} (100 - \% \text{ZnO})} \right] \times 100 \quad (6)$$

where %ZnO is the percentage of ZnO cycles and ρ_{Zn} and ρ_{Al} are the densities of Zn and Al atoms deposited during each ALD cycle for the pure ZnO and Al₂O₃ films, respectively. The measured Zn film content matches the expected values for ZnO cycle percentages above 90%. For lower ZnO cycle percentages, the Zn film content is far below the expected values predicted by the “rule of mixtures” formula.

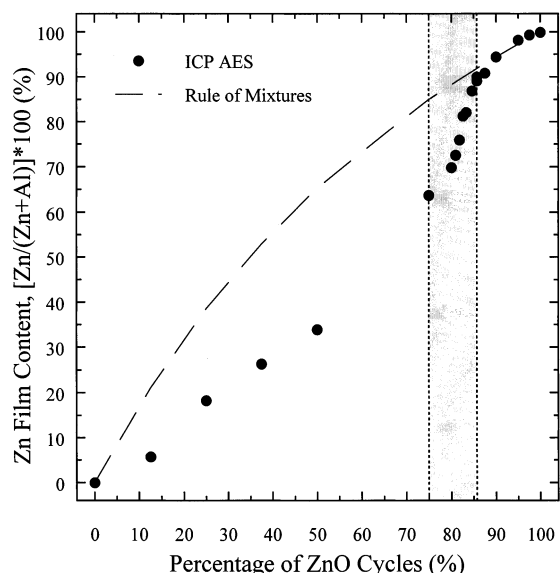


Figure 7. Zn film content versus percentage of ZnO cycles used to grow the ZnO/Al₂O₃ alloy film. The Zn film content was determined using inductively coupled plasma (ICP) atomic emission spectroscopy (AES).

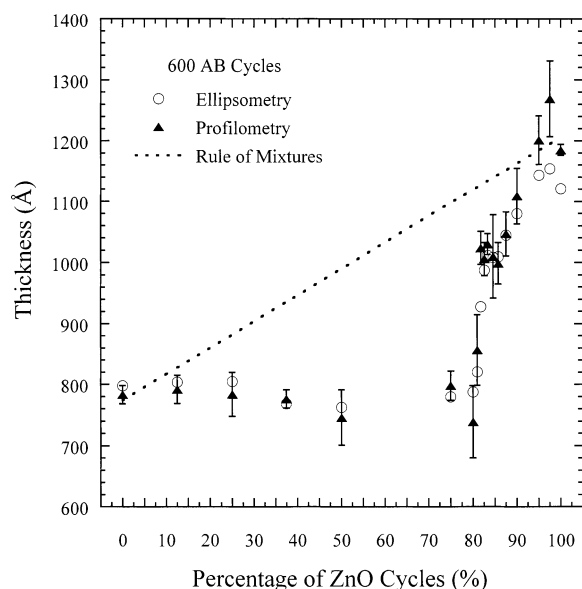


Figure 8. Thickness after 600 AB cycles versus percentage of ZnO cycles used to grow ZnO/Al₂O₃ alloy films. The film thickness was measured using ellipsometry (open circles) and stylus profilometry (solid triangles).

Figure 8 shows the thicknesses of the ZnO/Al₂O₃ alloy films prepared using 600 ALD cycles while varying the ZnO cycle percentage. The error bars on the solid triangles represent the standard deviation of 3–5 separate stylus profilometry measurements at different locations on each of the ZnO/Al₂O₃ alloy films. The growth rate of the ZnO/Al₂O₃ alloy films is relatively constant from 0% to ~70% ZnO cycle percentage. The growth rate then increases sharply between 80% and 100% ZnO cycle percentage. The dashed line in Figure 8 represents the expected thicknesses for the alloy films using the “rule of mixtures” formula

$$600 \text{ Cycles} \times [(2.01 \text{ Å/cycle})\% \text{ZnO} + (1.29 \text{ Å/cycle})(100 - \% \text{ZnO})]/100 \quad (7)$$

For ZnO cycle percentages between ~10 and 90%, the alloy film thicknesses are lower than the expected values predicted by the “rule of mixtures” formula.

In situ QCM measurements were performed during the deposition of the ZnO/Al₂O₃ alloy films and the results are shown in Figure 9. The open circles in Figure 9 represent the incremental mass changes recorded during each DEZ/H₂O cycle, and the solid circles show the mass added during each TMA/H₂O cycle. The dashed and solid lines show the average ALD growth rates of 113 ng/cm²/cycle and 37.6 ng/cm²/cycle measured for the pure ZnO and Al₂O₃ films, respectively, from Figure 5. The QCM data for the ZnO/Al₂O₃ alloy films was recorded after 10–20 cycles of ALD at the specified ZnO cycle percentage to allow the QCM data to achieve a steady-state pattern. QCM measurements were also recorded for additional ZnO cycle percentages that are not shown in Figure 9.

For many of the QCM measurements shown in Figure 9, the ALD growth rates are below the growth rates for pure ZnO and Al₂O₃ ALD as indicated by the dashed and solid lines, respectively. For instance, for the film grown using a ZnO cycle percentage of 50% shown by Figure 9d, each Al₂O₃ cycle deposits ~10 ng/cm² and each ZnO cycle deposits ~75 ng/cm². These growth rates are only 27% and 67% of the corresponding growth rates during pure ZnO and Al₂O₃ ALD. More surprisingly, the Al₂O₃ cycles for films grown using ZnO cycle percentages of 75 and 85% indicate negative growth rates of –50 and –10 ng/cm²/cycle, respectively. Negative growth, or etching, was observed by the QCM measurements over a range of ZnO cycle percentages from 75–86%. The range of ZnO cycle percentages where etching was observed during the Al₂O₃ cycles is indicated by the gray region in Figure 7.

Figure 10 presents additional information on the etching during Al₂O₃ ALD cycles. The QCM data recorded during eight ALD cycles for the alloy film grown using a ZnO cycle percentage of 75% are shown in Figure 10. The solid line presents the mass deposited versus time measured by the QCM. The status of the TMA, H₂O, and DEZ dosing valves are indicated at the bottom of the figure. Figure 10 demonstrates that a reduction in mass occurs during each TMA exposure of each Al₂O₃ cycle. The subsequent H₂O exposure adds a small amount of mass to the film.

IV. Discussion

A. ALD of Pure ZnO and Al₂O₃ Films. Figure 3 shows that the ellipsometry and profilometry measurements are consistent with average growth rates of 2.01 Å/cycle for ZnO ALD and 1.29 Å/cycle for Al₂O₃ ALD. The average growth rate of 2.01 Å/cycle for ZnO ALD agrees well with the value of 2.1 Å/cycle measured recently under similar conditions.⁴¹ A growth rate of 1.1 Å/cycle was measured previously for Al₂O₃ ALD at 177 °C.⁴² However, this previous investigation used H₂O exposures with lower pressures than those used in the current study. The growth rate for Al₂O₃ ALD has been shown to saturate at larger values using higher H₂O pressures.⁴⁶

Figure 4 demonstrates a short nucleation period for Al₂O₃ ALD. The ellipsometry measurements show that the Al₂O₃ ALD growth rate increases from ~1.05 Å/cycle

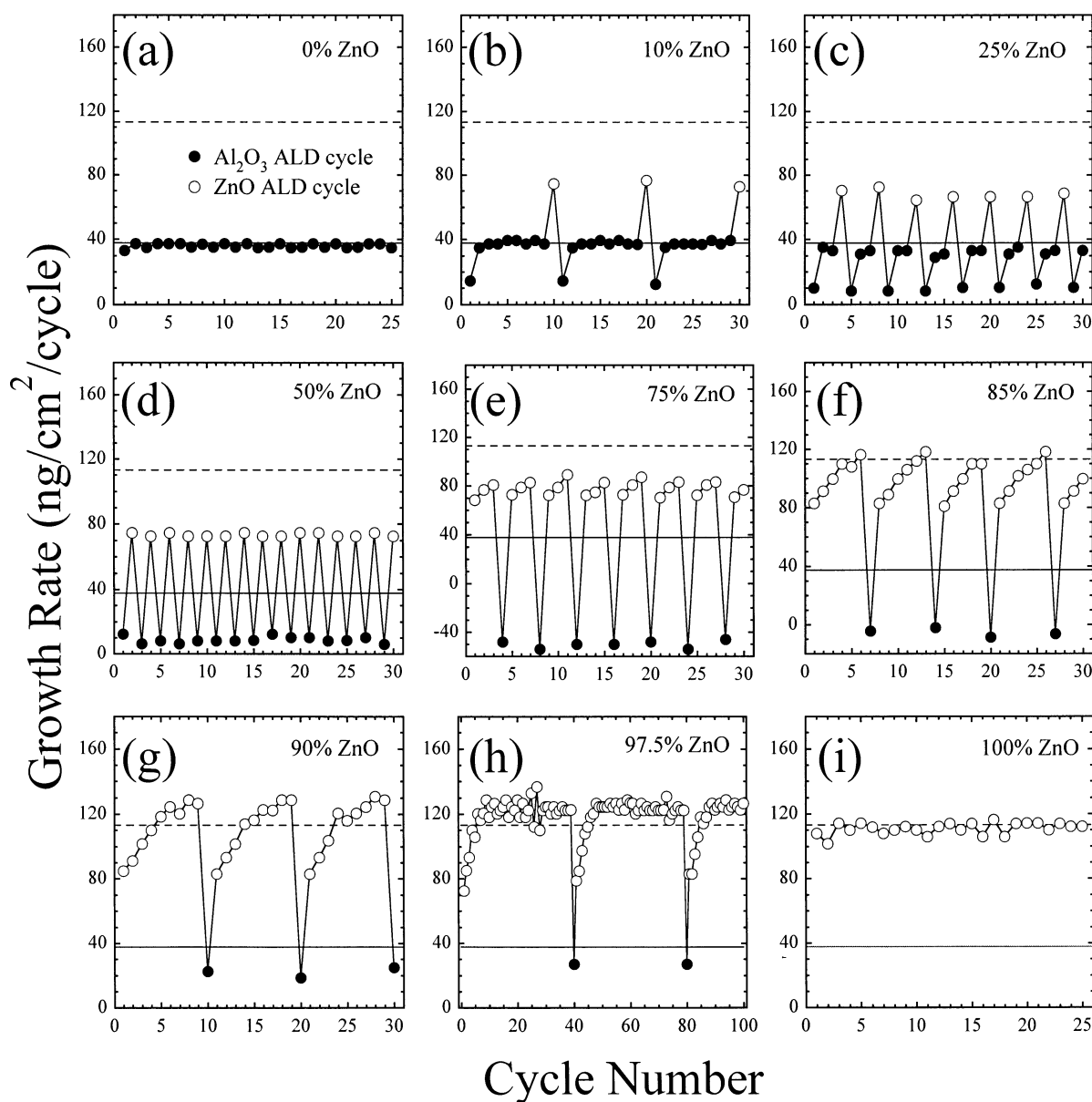


Figure 9. Growth rates obtained from in situ QCM measurements during the ALD of various ZnO/Al₂O₃ alloy films prepared using different percentages of ZnO cycles. The horizontal dashed and solid lines show the average ALD growth rates measured for pure ZnO and Al₂O₃, respectively.

at 25 AB cycles to ~ 1.29 Å/cycle above 100 AB cycles. This nucleation period results from a reduced TMA reactivity on the HF-etched Si(100) substrate due to the absence of surface hydroxyl groups as has been observed previously.⁴⁸ Larger TMA and H₂O exposures may shorten the Al₂O₃ ALD nucleation period. Verifying the Al₂O₃ nucleation period using the stylus profilometer was not possible because the stylus profilometer is not sufficiently sensitive to record thicknesses ≤ 100 Å.

The ZnO growth rate in Figure 4 also exhibits a nucleation period. The ZnO ALD growth rate is ~ 1.5 Å/cycle initially and increases to 2.01 Å/cycle following 700–900 AB cycles. Similarly to Al₂O₃ ALD, surface hydroxyls facilitate the ZnO ALD surface chemistry. There are no hydroxyls on the HF-etched Si(100)

substrate and the DEZ reactivity is low. A similar effect was observed during previous QCM investigations of ZnO ALD.⁴¹ In this previous study, ~ 100 AB cycles were required to achieve a steady-state ZnO ALD growth rate of 2.1 Å/cycle on a gold-coated QCM surface.⁴¹ Larger initial DEZ and H₂O exposures may help to facilitate more rapid ZnO ALD nucleation.

Alternatively, the ZnO nucleation period may reflect the slow evolution of ZnO nanocrystals. The surface roughness and surface area of the ZnO ALD films increase with the number of AB cycles.⁶ The reactivity of the ZnO nanocrystals may also increase with crystal size. Consequently, the steady-state ZnO ALD growth rate of 2.01 Å/cycle may not be reached until the ZnO nanocrystals have grown to a certain size. Changes in growth rate with film thickness have also been observed during TiO₂ ALD.⁴⁹ The TiO₂ ALD growth rate was observed to decrease slowly from 0.62 Å/cycle at 1000 cycles to 0.45 Å/cycle at 10 000 cycles. This decrease was

(48) Gosset, L. G.; Damlencourt, J.-F.; Renault, O.; Rouchon, D.; Holliger, P.; Ermolie, A.; Trimaille, I.; Ganem, J.-J.; Martin, F.; Semeria, M.-N. *J. Non-Cryst. Solids* **2002**, *303*, 17.

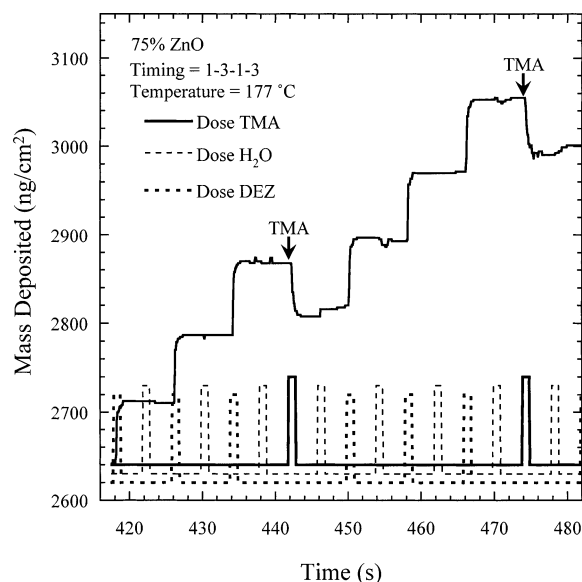


Figure 10. QCM measurements of mass deposited versus time during the ALD of a ZnO/Al₂O₃ alloy film grown using a ZnO cycle percentage of 75%.

believed to result from a slow change in morphology of the crystalline surface with film thickness.

The QCM mass measurements in Figure 5 can be combined with the film thickness measurements in Figure 3 to determine the densities for the ZnO and Al₂O₃ ALD films. The ZnO ALD growth rates of 113 ng/cm²/cycle from Figures 5 and 2.01 Å/cycle from Figure 3 yield a ZnO ALD density of 5.62 g/cm³. Similarly, the Al₂O₃ ALD growth rates of 37.6 ng/cm²/cycle from Figures 5 and 1.29 Å/cycle from Figure 3 yield an Al₂O₃ ALD density of 2.91 g/cm³.

The measured ZnO ALD density of 5.62 g/cm³ is in excellent agreement with the literature value of 5.61 g/cm³.⁵⁰ The measured Al₂O₃ density of 2.91 g/cm³ is slightly lower than a previous estimate of 3.5 g/cm³ for the density of Al₂O₃ ALD films.⁴² This estimate was obtained from refractive index measurements using the Lorentz–Lorenz relationship and is close to the accepted value of 3.5–3.9 g/cm³ for γ -Al₂O₃.⁵⁰ Recent X-ray reflectivity measurements performed on Al₂O₃ ALD films prepared in the viscous flow ALD reactor yield a density of 3.1 ± 0.1 g/cm³.⁵¹ This density is in reasonable agreement with the density of 2.91 g/cm³ obtained in this study.

The average numbers of hydroxyl groups reacting with each DEZ or TMA molecule during ZnO and Al₂O₃ ALD are important for analyzing the surface chemistry during ZnO/Al₂O₃ alloy growth. These quantities can be extracted from the QCM pulse shapes in Figure 6. The half reactions for ZnO and Al₂O₃ ALD given by eqs 1–4 can be rewritten to allow a variable number of hydroxyl groups, n , and these new equations can be rearranged to yield the ratio of mass changes occurring during the A and B half reactions.⁵² For ZnO ALD, the QCM mass ratio is

$$\frac{\Delta M_B}{\Delta M_A} = \frac{(30)n - 42}{124 - (30)n} \quad (8)$$

From the mass changes shown in Figure 6a, $\Delta M_B/\Delta M_A = -0.0061$ and $n = 1.37$. Similarly, the QCM mass ratio for Al₂O₃ ALD is

$$\frac{\Delta M_B}{\Delta M_A} = \frac{(16)n - 21}{72 - (16)n} \quad (9)$$

From Figure 6b, $\Delta M_B/\Delta M_A = 0.053$ and $n = 1.47$. A value of $n \sim 1.5$ was calculated previously for Al₂O₃ ALD under conditions similar to the conditions employed in this study.⁵² In addition, the QCM pulse shapes in Figure 6a and b resemble previous measurements for ZnO⁴¹ and Al₂O₃ ALD,⁵² respectively.

B. Etching During ALD of ZnO/Al₂O₃ Alloy Films. Figure 7 demonstrates that the Zn film content in the ZnO/Al₂O₃ alloy films is significantly below many of the values predicted by the “rule of mixtures” formula. In addition, a pronounced drop in Zn film content below the predicted values is observed between ~75 and 86% ZnO. This Zn deficiency may be attributed, in part, to the reduced initial reactivity of DEZ on the TMA-reacted surface as discussed in Section IV C. However, the QCM measurements reveal a negative growth rate during the Al₂O₃ ALD cycles for films deposited using ZnO cycle percentages of 75–86%. Some of these negative growth rates are illustrated in Figure 9e and f. These negative growth rates suggest that etching occurs during the Al₂O₃ ALD cycles.

Further information regarding the etching process is evident in Figure 10. Figure 10 reveals that a mass loss of ~62 ng/cm² occurs with each TMA exposure during the growth of the alloy film using a ZnO cycle percentage of 75%. One possible surface reaction to explain this mass loss is



Equation 10 predicts a mass loss of -23.4 g/mol. Assuming a density of surface zinc atoms of $\sim 10^{15}$ cm⁻², eq 10 predicts a mass loss of approximately -40 ng/cm². This mass loss is in reasonable agreement with the observed mass loss of -62 ng/cm².

Etching of metal oxide films during ALD has been observed previously using metal chlorides. For instance, TaCl₅ has been observed to etch Ta₂O₅ ALD films in QCM studies performed at 400 °C.⁵³ Organometallic reagents, such as β -diketonates, can also etch metal oxide surfaces. QCM studies have revealed the etching of the SrO ALD surface by the Sr(thd)₂ precursor at 240 °C.⁵⁴ Furthermore, β -diketonate complexes can selectively remove metal atoms from a mixed metal oxide surface. In an ALD study of the growth of MgMnCoO mixed oxide films, Mg(thd)₂ and Mn(thd)₂ were shown to remove ~ 0.25 Co atoms/nm²/cycle.²⁹

(49) Ritala, M.; Leskela, M.; Nykanen, E.; Soininen, P.; Niinisto, L. *Thin Solid Films* **1993**, *225*, 288.

(50) Weast, R. C.; Astle, M. J. *CRC Handbook of Chemistry and Physics*, 63rd ed.; CRC Press: Boca Raton, FL, 1982–1983.

(51) Jensen, J. M.; Oelkers, A. B.; Toivola, R.; Johnson, D. C.; Elam, J. W.; George, S. M. *Chem. Mater.* **2002**, *14*, 2276.

(52) Rahtu, A.; Alaranta, T.; Ritala, M. *Langmuir* **2001**, *17*, 6506.

(53) Aarik, J.; Aidla, A.; Kukli, K.; Uustare, T. *J. Cryst. Growth* **1994**, *114*, 116.

(54) Aarik, J.; Aidla, A.; Jaek, A.; Leskela, M.; Niinisto, L. *J. Mater. Chem.* **1994**, *4*, 1239.

Although ZnO etching by TMA has not been previously reported, earlier studies have reported the dry etching of ZnO in a CH₄ plasma.⁵⁵ The driving force for this etching process was believed to be the formation of Zn(CH₃)₂. CH₄ produced by the reaction of TMA with the hydroxylated ZnO surface may abstract Zn to form Zn(CH₃)₂. The dissociative adsorption of CH₄ on ZnO is highly exothermic and the activation energy is calculated to be -81 kcal/mol.⁵⁶ The transfer of CH₃ groups from Al to Zn may also occur without the intermediate formation of CH₄.

An additional driving force for Zn etching may be the formation of the ZnAl₂O₄ spinel. This spinel is thermodynamically stable. The enthalpy for the reaction ZnO + Al₂O₃ → ZnAl₂O₄ is -43.3 kcal/mol.⁵⁷ The ZnAl₂O₄ spinel has a Zn content of 33%. Removal of Zn from the ZnO/Al₂O₃ alloy films with Zn film content >33% may promote the formation of the spinel phase. Figure 10 shows that the Zn etching is observed within a narrow range of composition between ~64 and 90% Zn. This behavior may reflect the formation of localized regions of the thermodynamically stable ZnAl₂O₄ spinel. Additional X-ray diffraction and transmission electron microscopy analysis could help to confirm these speculations.

C. Nucleation During ALD of ZnO/Al₂O₃ Alloy Films. The measured thicknesses for many of the ZnO/Al₂O₃ alloy films in Figure 8 are significantly below the thicknesses predicted using the "rule of mixtures" formula in eq 7. One explanation for the lower than expected alloy film thicknesses is that a finite number of cycles is required for ZnO to nucleate on Al₂O₃ or Al-doped ZnO surfaces and for Al₂O₃ to nucleate on ZnO or Zn-doped Al₂O₃ surfaces. During the nucleation periods, the ALD growth rates gradually increase and progressively reach their bulk values. Figure 9f-h supports this explanation. Following one or more TMA pulses, 4-6 cycles of ZnO ALD are required to reach the bulk ZnO ALD growth rate of 113 ng/cm²/cycle. In addition, Figure 9b and c indicates that 2-3 cycles of Al₂O₃ ALD are required to reach the bulk Al₂O₃ ALD growth rate of 37.6 ng/cm²/cycle following DEZ exposures.

The reduced initial growth rate when making the transition between ZnO ALD and Al₂O₃ ALD results in an average growth rate that is significantly lower than the "rule of mixtures" prediction. For example, the average ZnO ALD growth rate is reduced to 61% of the bulk value and the average Al₂O₃ ALD growth rate is reduced to 68% of the bulk value during the growth of the alloy film using a ZnO cycle percentage of 25% as shown in Figure 9c. Interestingly, these QCM growth rates underestimate the measured film thicknesses. Equation 7 with these reduced growth rates predicts a film thickness of 579 Å for a film grown using a ZnO cycle percentage of 25%. In contrast, the measured thickness in Figure 8 is ~790 Å. This difference must result from a film density that is lower than the density predicted by a "rule of mixtures" formula for density.

Periods of reduced growth during nucleation are commonly observed during the ALD of composite films.^{1,19,27,30,31,37} The reduced growth rates are believed to result from a lower number of reactive sites²⁷ or a reduced reactivity for the reactive sites.^{19,30,31,37} In the present study, the reduced Al₂O₃ growth rate following DEZ pulses could result from a deficiency of surface hydroxyl groups. The Al₂O₃ ALD growth rate is known to decrease at higher temperature because of the lower surface hydroxyl coverage.⁴² The hydroxyl coverage on amorphous Al₂O₃ surfaces is $\Theta_{\text{OH}} \sim 0.94 \times 10^{15} \text{ cm}^{-2}$ at 177 °C.⁵⁸⁻⁶⁰ In contrast, the hydroxyl coverage is estimated to be $\Theta_{\text{OH}} \sim 1.06 \times 10^{15} \text{ cm}^{-2}$ on ZnO(100) at 177 °C.^{61,62} If hydroxyl coverages alone dictated the ALD growth rates, then Al₂O₃ ALD would occur ~13% faster on ZnO than on Al₂O₃. Because the opposite trend is observed following DEZ pulses, other factors must dictate the reduced ALD growth rates.

A similar argument applies for ZnO ALD following TMA pulses. On average, DEZ reacts with $n = 1.37$ hydroxyl groups while TMA reacts with $m = 1.47$ hydroxyl groups. Because the hydroxyl coverages are nearly equivalent on Al₂O₃ and ZnO at 177 °C, DEZ and TMA should react nearly equally with these two surfaces. However, Figure 9b and c shows that DEZ reactivity is reduced by ~30% on the Al₂O₃ surface. These results argue that hydroxyl coverage alone does not dominate the growth rates during the ALD of the ZnO/Al₂O₃ alloy films.

An alternative explanation for some of the effects observed during the ALD growth of ZnO/Al₂O₃ alloy films relates to the relative acidity of the ZnO and Al₂O₃ surfaces. The ZnO surface is basic and has an isoelectric point of pH 9.5 in water.⁶³ The Al₂O₃ ALD films have a density similar to that of γ -Al₂O₃. The γ -Al₂O₃ surface is nearly neutral and has an isoelectric point of pH 7.0-7.5 in water.^{64,65} During the transition between ZnO and Al₂O₃, the ZnO and Al₂O₃ hydroxyls will coexist on the alloy film surface. This coexistence may allow a proton exchange surface reaction to occur:



Formation of the ZnOH₂⁺...AlO⁻* complex might deactivate the surface hydroxyl groups and render them less reactive to the TMA and DEZ reactants. In situ Fourier transform infrared (FTIR) investigations⁶⁶ of ZnO/Al₂O₃ alloy ALD could observe the surface species proposed in eq 11 and would help to evaluate this model.

Although the TMA pulses initially lower the ZnO growth rate for 4-6 cycles, the ZnO growth rate subsequently increases to ~120-130 ng/cm² as shown

(55) Lee, J.-M.; Chang, K. M.; Kim, K.-K.; Choi, W.-K.; Park, S.-J. *J. Electrochem. Soc.* **2001**, *148*, G1.

(56) Zhanpeisov, N. U.; Zhidomirov, G. M.; Baerns, M. *J. Mol. Catal. A: Chem.* **1995**, *99*, 35.

(57) Pandey, R.; Gale, J. D.; Sampath, S. K.; Recio, J. M. *J. Am. Ceram. Soc.* **1999**, *82*, 3337.

(58) Peri, J. B. *J. Phys. Chem.* **1965**, *69*, 211.

(59) Peri, J. B. *J. Phys. Chem.* **1965**, *69*, 220.

(60) Dillon, A. C.; Ott, A. W.; Way, J. D.; George, S. M. *Surf. Sci.* **1995**, *322*, 230.

(61) Atherton, K.; Newbold, G.; Hockey, J. A. *Discuss. Faraday Soc.* **1971**, *52*, 33.

(62) Mattmann, G.; Oswald, H. R.; Schweizer, F. *Helv. Chim. Acta* **1972**, *55*, 1249.

(63) Topoglidis, E.; Cass, A. E. G.; O'Regan, B.; Durrant, J. R. *J. Electroanal. Chem.* **2001**, *517*, 20.

(64) Baohong, L.; Hu, R.; Deng, J. *Anal. Chim. Acta* **1997**, *341*, 161.

(65) Schaep, J.; Vandecasteele, C.; Peeters, B.; Luyten, J.; Dotremont, C.; Roels, D. *J. Membr. Sci.* **1999**, *163*, 29.

(66) Ferguson, J. D.; Weimer, A. W.; George, S. M. *Appl. Surf. Sci.* **2000**, *162-163*, 280.

in Figure 9g and h. This growth rate is larger than the bulk ZnO ALD growth rate of 113 ng/cm². Figure 9h demonstrates that this enhanced ZnO ALD growth rate following the renucleation of ZnO after a TMA pulse can persist for at least 39 cycles. The enhanced ZnO ALD growth rate is also observed in the ex situ film thickness measurements. Figure 8 shows that the films grown using a ZnO cycle percentage of 97.5% are 3–7% thicker than the ZnO films grown using a ZnO cycle percentage of 100%.

This enhanced growth rate at very low atomic percentages of aluminum may correlate with the film conductivity. Small amounts of Al dopants in ZnO are known to increase the ZnO film conductivity.^{38,67,68} Higher ZnO conductivities may increase the nucleophilic character of the hydroxyl groups and increase the surface reactivity. In situ resistivity⁶⁹ and FTIR measurements⁶⁶ performed during the ALD of ZnO/Al₂O₃ alloy films may clarify the relationship between conductivity and hydroxyl group reactivity.

V. Conclusions

A set of ZnO/Al₂O₃ alloy films was prepared using atomic layer deposition (ALD) techniques. The ZnO/Al₂O₃ alloy composition was adjusted by varying the percentage of ZnO ALD cycles from 0 to 100%. Many of

the ZnO/Al₂O₃ alloy films were thinner and contained less Zn than expected based on “rule of mixtures” predictions. To investigate these discrepancies, in situ quartz crystal microbalance (QCM) measurements were performed during the ALD of the ZnO/Al₂O₃ alloy films. The QCM measurements revealed that the lower than expected Zn content may result from the etching of Zn by trimethyl aluminum during the Al₂O₃ ALD cycles. In addition, the QCM data indicated that the unexpectedly low thicknesses were caused by reduced initial growth rates for ZnO ALD on Al₂O₃ or Al-doped ZnO surfaces and Al₂O₃ ALD on ZnO or Zn-doped Al₂O₃ surfaces. Understanding the mechanisms of ALD alloy film growth will facilitate the nanoengineering of novel composite films with tunable properties.

Acknowledgment. This work was funded by the Air Force Office of Scientific Research. Additional funding was supplied by Nanomaterials Research LLC in Longmont, CO. John Drexler of the Department of Geological Sciences at the University of Colorado performed the ICP–AES elemental analysis of the alloy films. We are grateful to Tom Seidel and Ofer Sneh of Genus, Inc. for donating some of the components needed to assemble the viscous flow ALD reactor.

CM020607+

(67) Sato, H.; Minami, T.; Takata, S.; Miyata, T.; Ishii, M. *Thin Solid Films* **1993**, 236, 14.

(68) Kim, H.; Pique, A.; Horwitz, J. S.; Murata, H.; Kafafi, Z. H.; Gilmore, C. M.; Chrisey, D. B. *Thin Solid Films* **2000**, 377–378, 798.

(69) Schuisky, M.; Elam, J. W.; George, S. M. *Appl. Phys. Lett.* **2002**, 88, 180.